Sum-frequency generation using strong-field coupling and induced transparency in atomic hydrogen

G. Z. Zhang, M. Katsuragawa, and K. Hakuta
Department of Applied Physics and Chemistry and Institute for Laser Science, University of Electro-Communications, Chofu, Tokyo 182, Japan

R. I. Thompson and B. P. Stoicheff
Department of Physics, University of Toronto, and Ontario Laser and Lightwave Research Centre, Toronto, Ontario, Canada M5S 1A7

(Received 17 March 1995)

The sum-frequency generation process using strong-field coupling and quantum interference is described systematically using atomic hydrogen both in theory and experiment. It is shown that strong coupling at the $3p$-$2s$ transition creates destructive interference to reduce the linear susceptibility at the resonant $3p \leftarrow 1s$ transition. Simultaneously, two-photon coupling of the $2s$ and $1s$ states produces constructive interference to resonantly enhance the nonlinear susceptibility for sum-frequency generation at the $3p \rightarrow 1s$ (Lyman-β) transition. Experimental results clearly demonstrate the theoretical predictions. When the Rabi frequency for the $3p$-$2s$ coupling exceeds the Doppler tail of the medium, the photoion signals on resonance are suppressed significantly because of induced transparency. The generated Lyman-β radiation grows rapidly by a factor of 250 at an atom density of 10^{15} cm^{-3} and interaction length of 3.5 cm, resulting in a conversion efficiency of 2×10^{-4}.

PACS number(s): 42.65.Ky, 32.80.Fb, 42.50.Hz, 42.50.Gy

I. INTRODUCTION

Nonlinear frequency up-conversion techniques using atomic media have been extensively investigated theoretically and experimentally in the past two decades for generating vacuum ultraviolet (vuv) to extreme ultraviolet (EUV) coherent radiation [1,2]. One important advantage of using a gas as a nonlinear medium is the sharp resonance enhancement of the nonlinear optical susceptibility, which can overcome the disadvantage arising from the low number density compared to a solid medium. However, when the generated wavelength is tuned to near resonance, the linear susceptibility will also show a rapid increase, although the nonlinear susceptibility can be enhanced many orders of magnitude. This increasing linear susceptibility seriously limits the conversion efficiency in the nonlinear generation process due to strong resonant absorption and phase mismatching.

In 1990, Harris, Field, and Imamoglu [3] proposed an idea to overcome this trade-off problem. The main point was to introduce a quantum interference in the nonlinear generation process. They have shown theoretically that, by strongly coupling a metastable state and an upper state of a resonant transition, the nonlinear susceptibility can be resonantly enhanced through constructive interference while the linear susceptibility is reduced in magnitude to zero through destructive interference. The destructive interference in the linear susceptibility renders an otherwise opaque medium transparent on resonance. This process is termed electromagnetically induced transparency (EIT) [4–6].

So far, several experimental works have been reported in terms of nonlinear optical generation using quantum interferences. Hakuta, Marmet, and Stoicheff [7–9] have extended the concept of the EIT effect to dc electric-field coupling using atomic hydrogen and have generated coherent, second-harmonic radiation at 121.6 nm. Hahn, King, and Harris [10] applied the quantum interference arising from the autoionizing Fano resonance to the sum-frequency generation using zinc vapor at 103 nm. They showed that, by properly choosing the intermediate state, it is possible to realize constructive and destructive interferences in nonlinear and linear susceptibilities, respectively, and obtained a high conversion efficiency of 1×10^{-3}. The control of linear susceptibility has also been investigated from the viewpoint of refractive index control [11], which can give another freedom to nonlinear optical generation process in terms of phase-matching control.

In a recent Letter [12], we reported a study of sum-frequency generation using strong-field coupling and induced transparency (EIT) in atomic hydrogen as a test medium. A strong laser field was applied to couple the $2s$ state with the upper $3p$ state and simultaneously a second laser field was applied to couple the $2s$ and the $1s$ levels through a two-photon process. In this way, the sum-frequency generation process occurring at the $3p \rightarrow 1s$ Lyman-β transition (102.6 nm) was investigated. It was demonstrated experimentally that the linear susceptibility can be reduced at the resonant center of the Lyman-β transition, when the laser coupling exceeded the Doppler tails of the two dressed states, while the nonlinear susceptibility can be enhanced with the resonance effect. The purpose of the present paper is to give a detailed description of the generation process using strong-field coupling and quantum interference in atomic hydrogen and to systematically compare the observed results with the theoretical predictions.

II. THEORY

A. Interaction formulation in dressed-state basis

Figure 1 illustrates the interaction scheme for the present study. Here, bare atomic hydrogen states of 1*s*, 2*s*, and 3*p* are denoted as $|1\rangle$, $|2\rangle$, and $|3\rangle$, respectively. A laser field termed ω_c is applied to strongly couple the state $|2\rangle$ with the upper state $|3\rangle$, resulting in a pair of dressed states $|2d\rangle$ and $|3d\rangle$. Another laser field denoted as ω_e is used for the two-photon coupling of the states $|1\rangle$ and $|2\rangle$. Sum-frequency generation occurs with a frequency $\omega_g=2\omega_e+\omega_c$ at the resonance $|3\rangle$-$|1\rangle$ transition. It should be noted that in the present scheme the laser fields must inevitably photoionize the upper states and open additional decay channels for the upper states.

The atom-field interaction in this scheme may be treated by calculating the single-atom probability amplitudes of the three levels using Schrödinger's equation. Here we formulate the interaction using the dressed states as a basis set. Under the present strong-coupling condition, this basis set can give a more comprehensive physical understanding of quantum interferences than the basis set of bare atomic states. Here the dressed-probability amplitude equations are obtained by transforming from the time-varying probability amplitude equations in the bare-state basis obtained from Schrödinger's equation [3]

$$\frac{db_1(t)}{dt}=\frac{j}{2}[\Omega_{12}b_2(t)+\Omega_{13}b_3(t)] , \tag{1a}$$

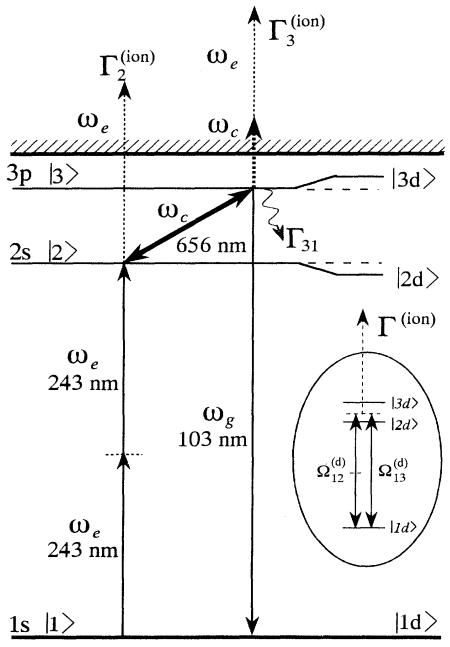

FIG. 1. Partial energy-level diagram of atomic hydrogen for the sum-frequency generation process using strong-field coupling and quantum interference. $\omega_g=2\omega_e+\omega_c$. The inset shows a diagram of the dressed-state basis.

$$\frac{db_2(t)}{dt}+j\Delta\tilde{\omega}_{21}b_2(t)=\frac{j}{2}[\Omega_{21}b_1(t)+\Omega_{23}b_3(t)] , \tag{1b}$$

$$\frac{db_3(t)}{dt}+j\Delta\tilde{\omega}_{31}b_3(t)=\frac{j}{2}[\Omega_{31}b_1(t)+\Omega_{32}b_2(t)] , \tag{1c}$$

where $\Omega_{13}=\mu_{13}E_g/\hbar$ and $\Omega_{23}=\mu_{23}E_c/\hbar$ are the respective one-photon Rabi frequencies of the generated radiation (ω_g) and the coupling field (ω_c). Ω_{12} is defined as an effective two-photon Rabi frequency for the field at ω_e; $\Omega_{12}=\alpha_{12}E_e^2/\hbar$, where $\alpha_{12}=\sum_i[\mu_{1i}\mu_{i2}/2\hbar(\omega_i-\omega_e)]$, and the μ_{ij} stand for the pertinent matrix elements. E_e, E_c, and E_g are the amplitudes of applied fields, respectively. The values for Ω_{23} and Ω_{12} are chosen to be real, positive values. The detunings $\Delta\tilde{\omega}_{21}=\omega_2-\omega_1-2\omega_e-j/2\Gamma_2$ and $\Delta\tilde{\omega}_{31}=\omega_3-\omega_1-\omega_g-j/2\Gamma_3$ include Γ_2 and Γ_3, the decay rates of states $|2\rangle$ and $|3\rangle$, respectively. Photoionization processes are phenomenologically included in the decay processes of the upper states.

Now we transform Eqs. (1) to equivalent expressions in the dressed-state basis. With the strong coupling between states $|2\rangle$ and $|3\rangle$, the transform from the bare-state basis to the dressed-state basis [1,4] may be written

$$|1d\rangle=|1\rangle , \tag{2a}$$

$$|2d\rangle=\cos\frac{\theta}{2}|2\rangle+\sin\frac{\theta}{2}|3\rangle , \tag{2b}$$

$$|3d\rangle=-\sin\frac{\theta}{2}|2\rangle+\cos\frac{\theta}{2}|3\rangle , \tag{2c}$$

where

$$\tan\theta=\frac{\Omega_{32}}{|\Delta|} , \tag{3a}$$

$$\Delta=\omega_3-\omega_2-\omega_c , \tag{3b}$$

$$0\le\theta\le\frac{\pi}{2} . \tag{3c}$$

We define the $|2d\rangle$ and $|3d\rangle$ states as symmetric and antisymmetric linear combinations of the bare states, respectively. By substituting Eqs. (2) and (3) into Eqs. (1), we may express the dressed-probability amplitude equations as

$$\frac{db_{1d}(t)}{dt}=\frac{j}{2}[\Omega_{12}^{(d)}b_{2d}(t)+\Omega_{13}^{(d)}b_{3d}(t)] , \tag{4a}$$

$$\frac{db_{2d}(t)}{dt}+j\Delta\tilde{\omega}_{2d}b_{2d}(t)=\frac{j}{2}\Omega_{21}^{(d)}b_{1d}(t)+\kappa b_{3d}(t) , \tag{4b}$$

$$\frac{db_{3d}(t)}{dt}+j\Delta\tilde{\omega}_{3d}b_{3d}(t)=\frac{j}{2}\Omega_{31}^{(d)}b_{1d}(t)+\kappa b_{2d}(t) , \tag{4c}$$

where

$$\Omega_{12}^{(d)}=\Omega_{12}\cos\frac{\theta}{2}+\Omega_{13}\sin\frac{\theta}{2} , \tag{5a}$$

$$\Omega_{13}^{(d)}=-\Omega_{12}\sin\frac{\theta}{2}+\Omega_{13}\cos\frac{\theta}{2} , \tag{5b}$$

$$\Delta\tilde{\omega}_{2d}=\omega_2-\omega_1+\delta-2\omega_e-\frac{j}{2}\Gamma_{2d} , \tag{5c}$$

$$\Delta\tilde{\omega}_{3d}=\omega_3-\omega_1-\delta-\omega_g-\frac{j}{2}\Gamma_{3d}\ , \tag{5d}$$

$$\kappa=-\tfrac{1}{4}(\Gamma_{3d}-\Gamma_{2d})\tan\theta$$
$$=-\tfrac{1}{4}(\Gamma_3-\Gamma_2)\sin\theta\ , \tag{5e}$$

and

$$\Gamma_{2d}=\Gamma_2\cos^2\frac{\theta}{2}+\Gamma_3\sin^2\frac{\theta}{2}\ , \tag{6a}$$

$$\Gamma_{3d}=\Gamma_2\sin^2\frac{\theta}{2}+\Gamma_3\cos^2\frac{\theta}{2}\ , \tag{6b}$$

$$\delta=\tfrac{1}{2}(|\Delta|-\sqrt{\Delta^2+\Omega_{32}^2})\ . \tag{6c}$$

Here $\Omega_{12}^{(d)}$ and $\Omega_{13}^{(d)}$ denote the Rabi frequencies for the $|1d\rangle$-$|2d\rangle$ and the $|1d\rangle$-$|3d\rangle$ transitions in the dressed-state basis; $\Delta\tilde{\omega}_{2d}$ and $\Delta\tilde{\omega}_{3d}$ represent the complex frequency detunings of dressed states $|2d\rangle$ and $|3d\rangle$, respectively; Γ_{2d} and Γ_{3d} are the decay rates of the two dressed states, respectively; and δ represents half of an effective Rabi splitting.

It should be mentioned in Eqs. (4b) and (4c) that the dressed probability amplitudes of b_{2d} and b_{3d} are coupled to each other through the κ term, which arises from the decay processes and is the origin of the quantum interferences. The interference appears destructively or constructively depending on the sign of κ value. If the κ value takes a minus sign, the decay of amplitude b_{2d} (b_{3d}) results in the driving of amplitude b_{3d} (b_{2d}), leading to destructive interference [13]. On the contrary, the plus κ value leads to constructive interference. Since $\sin\theta$ is always a positive value, the sign of κ is determined by the relation between the decay rates of the upper bare states as seen in Eq. (5e).

B. EIT and optical susceptibilities

From the viewpoint of single-atom response, the macroscopic polarization induced at the generated frequency ω_g can be expressed through the probability amplitudes of the dressed states as

$$P(t)=2N\,\mathrm{Re}\left\{\mu_{31}\left[\sin\frac{\theta}{2}b_{2d}^*+\cos\frac{\theta}{2}b_{3d}^*\right]b_{1d}e^{j\omega_g t}\right\}\ , \tag{7}$$

where N denotes the atom density. From the viewpoint of macroscopic optical response, the polarization may be described through optical susceptibilities. Here we define the dressed linear and nonlinear susceptibilities $\chi_D^{(L)}(-\omega_g,\omega_g)$ and $\chi_D^{(\mathrm{NL})}(-\omega_g,\omega_e,\omega_e)$, for the present scheme through the following expression for the polarization:

$$P(t)=\mathrm{Re}\{\varepsilon_0[\chi_D^{(L)}(-\omega_g,\omega_g)E_g+\tfrac{1}{2}\chi_D^{(\mathrm{NL})}(-\omega_g,\omega_e,\omega_e)E_e^2]e^{j\omega_g t}\}\ . \tag{8}$$

It should be mentioned that the strong-coupling field does not explicitly appear in the expression of polarization, which is involved in the susceptibilities. Assuming large decay rates for the two upper dressed states, we can readily obtain the probability amplitudes b_{2d} and b_{3d} as the stationary solutions

$$b_{2d}=\frac{\Omega_{21}^{(d)}\Delta\tilde{\omega}_{3d}-j\Omega_{31}^{(d)}\kappa}{2(\Delta\tilde{\omega}_{2d}\Delta\tilde{\omega}_{3d}+\kappa^2)}b_{1d}\ , \tag{9a}$$

$$b_{3d}=\frac{\Omega_{31}^{(d)}\Delta\tilde{\omega}_{2d}-j\Omega_{21}^{(d)}\kappa}{2(\Delta\tilde{\omega}_{2d}\Delta\tilde{\omega}_{3d}+\kappa^2)}b_{1d}\ . \tag{9b}$$

Substituting Eqs. (9) in Eq. (7) and using $|b_{1d}|^2=1$, we obtain, for the dressed susceptibilities

$$\chi_D^{(L)}(-\omega_g,\omega_g)=\frac{N|\mu_{13}|^2}{\varepsilon_0\hbar}\left[\frac{\Delta\tilde{\omega}_{2d}^*\cos^2\frac{\theta}{2}+\Delta\tilde{\omega}_{3d}^*\sin^2\frac{\theta}{2}+j\kappa\sin\theta}{\Delta\tilde{\omega}_{2d}^*\Delta\tilde{\omega}_{3d}^*+\kappa^2}\right]\ , \tag{10a}$$

$$\chi_D^{(\mathrm{NL})}(-\omega_g,\omega_e,\omega_e)=\frac{N\mu_{13}\alpha_{21}}{\varepsilon_0\hbar^2}\left[\frac{(\Delta\tilde{\omega}_{3d}^*-\Delta\tilde{\omega}_{2d}^*)\sin\theta+2j\kappa\cos\theta}{\Delta\tilde{\omega}_{2d}^*\Delta\tilde{\omega}_{3d}^*+\kappa^2}\right]\ . \tag{10b}$$

The third terms of the susceptibilities represent interference effects arising from the coupled decay processes of the two dressed states $|2d\rangle$ and $|3d\rangle$. By rewriting the decay parameters of the dressed states using those of the bare states, we can reach the expressions for the susceptibilities

$$\chi_D^{(L)}(-\omega_g,\omega_g)=\frac{N|\mu_{13}|^2}{\varepsilon_0\hbar}\left[\frac{\Delta\omega_{2d}\cos^2\frac{\theta}{2}+\Delta\omega_{3d}\sin^2\frac{\theta}{2}+j\frac{\Gamma_2}{2}}{\Delta\tilde{\omega}_{2d}^*\Delta\tilde{\omega}_{3d}^*+\kappa^2}\right]\ , \tag{11a}$$

$$\chi_D^{(\mathrm{NL})}(-\omega_g,\omega_e,\omega_e)=\frac{N\mu_{13}\alpha_{21}}{\varepsilon_0\hbar^2}\left[\frac{(\Delta\omega_{3d}-\Delta\omega_{2d})\sin\theta}{\Delta\tilde{\omega}_{2d}^*\Delta\tilde{\omega}_{3d}^*+\kappa^2}\right]\ . \tag{11b}$$

It is readily seen from Eq. (11a) that, if Γ_2 takes the value zero, the linear susceptibility $\chi_D^{(L)}(-\omega_g,\omega_g)$ becomes zero at the split center of two dressed states, where $\Delta\omega_{2d}\cos^2(\theta/2)+\Delta\omega_{3d}\sin^2(\theta/2)=0$ is satisfied. We should note that the Γ_3 term does not explicitly appear in Eq. (11a) due to the destructive interference. The effect of large broadening arising from the Γ_3 term is canceled for $\chi_D^{(L)}(-\omega_g,\omega_g)$ at the split center of two dressed states. This means that the absorption $\mathrm{Im}[\chi_D^{(L)}(-\omega_g,\omega_g)]$ can largely be reduced at the center, if the Γ_2 value is kept

small compared to Γ_3.

Such destructive interference does not appear in the nonlinear susceptibility. As seen from Eq. (11b), the dressed nonlinear susceptibility consists of two path contributions through the two dressed states with different sign, leading to constructive interference in the nonlinear susceptibility at the split center. In combination with the destructive interference in $\chi_D^{(L)}$ and the constructive interference in $\chi_D^{(\mathrm{NL})}$, the present sum-frequency generation process can satisfy simultaneously the essential conditions for obtaining high-conversion efficiencies.

C. Photoionization

Although the photoionization process may open new decay channels for the upper states and impose a limitation on the experimental parameters, one can obtain useful information of the reduced absorption through its spectra. The photoionization characteristics can be calculated theoretically through Eqs. (4). Substituting the stationary solutions of Eqs. (9) into Eq. (4a), we obtain

$$\frac{d|b_{1d}(t)|^2}{dt} = -\Gamma^{(\mathrm{ion})}|b_{1d}(t)|^2 . \tag{12}$$

Here we have defined the photoionization rate of the whole atomic system $\Gamma^{(\mathrm{ion})}$ as the decay rate of the ground-state population. It is easily understood that this is a reasonable definition because the strong-coupling achieves a stationary condition for the upper states and the population can escape from the system only through the photoionization processes. We have neglected the effect of population returning back to the ground state through the spontaneous-emission process, since we assume that the photoionization rate far exceeds the spontaneous-emission decay rate. The ionization rate $\Gamma^{(\mathrm{ion})}$ may be written as

$$\Gamma^{(\mathrm{ion})} = -\frac{1}{2}\mathrm{Im}\left[\frac{|\Omega_{12}^{(d)}|^2\Delta\tilde{\omega}_{3d}^* + |\Omega_{13}^{(d)}|^2\Delta\tilde{\omega}_{2d}^* + 2j\,\mathrm{Re}[\Omega_{12}^{(d)}\Omega_{31}^{(d)}\kappa]}{\Delta\tilde{\omega}_{2d}^*\Delta\tilde{\omega}_{3d}^* + \kappa^2}\right] . \tag{13}$$

The ionization rate $\Gamma^{(\mathrm{ion})}$ consists of three terms. The first and second terms show the effective excitations from two channels of $\Omega_{12}^{(d)}$ and $\Omega_{13}^{(d)}$ through $|2d\rangle$ and $|3d\rangle$, respectively. The last term gives an additional contribution from the ionization process induced by the interference between two excitation channels. Apparently, Eq. (13) gives the spectral profile of photoionization versus laser tuning. It should be noted that Eq. (13) leads to the same expression as that for $\chi_D^{(L)}$ in Eq. (11a) under the strong-coupling condition, if $\Omega_{12}^{(d)}$ and $\Omega_{13}^{(d)}$ become equal, i.e., in terms of the bare state parameters, if Ω_{13} far exceeds Ω_{12}. This is the reason why we can get information on the reduced absorption from the photoionization spectra.

D. Procedures for numerical calculation

Theoretical predictions were calculated numerically through the following procedures. The coupling laser frequency was fixed to the $3p$-$2s$ resonance and the bare states of the hydrogen atom were written as expressions of $|n,l,m_l\rangle$, namely, $|1\rangle=|1,0,0\rangle$, $|2\rangle=|2,0,0\rangle$, and $|3\rangle=|3,1,1\rangle$. A linearly polarized laser field coupled the $|2\rangle$ and $|1\rangle$ states, while σ^+-circular polarization was used to couple states $|3\rangle$ and $|2\rangle$. Energies of states $1s$, $2s$, and $3p$ are $\omega_1=0\ \mathrm{cm}^{-1}$, $\omega_2=822\,459.25\ \mathrm{cm}^{-1}$, and $\omega_3=97\,492.26\ \mathrm{cm}^{-1}$, respectively [14]. Spin-orbit interaction was neglected in the present treatment by assuming a much larger value of Ω_{23} than the spin-orbit splitting of $0.1\ \mathrm{cm}^{-1}$ for the $3p$ state.

The photoionization rates $\Gamma_2^{(\mathrm{ion})}$ and $\Gamma_3^{(\mathrm{ion})}$ of the bare states $|2\rangle$ and $|3\rangle$ were obtained by calculating the photoionization cross-sections using the tables of Burgess [15], giving

$$\Gamma_2^{(\mathrm{ion})} = 7.8\times10^6 I_{243}\ \mathrm{s}^{-1} , \tag{14a}$$

$$\Gamma_3^{(\mathrm{ion})} = 8.0\times10^7 I_{656} + 0.22\times10^7 I_{243}\ \mathrm{s}^{-1} , \tag{14b}$$

where I_{656} and I_{243} represent the intensities of the coupling and two-phonon fields measured in $\mathrm{MW\,cm}^{-2}$, respectively. The above expressions reveal that the photoionization plays an important role for the decay processes of the two upper states: At an intensity higher than 2 $\mathrm{MW\,cm}^{-2}$ for the coupling beam, the photoionization rate of state $|3\rangle$ exceeds the spontaneous emission rate of state $|3\rangle$, $1.6\times10^8\ \mathrm{s}^{-1}$ [16], and thus governs the decay process of the upper states. It should be mentioned that the photoionization cross section of state $|2\rangle$ at 243 nm is one order of magnitude smaller than that of state $|3\rangle$ at 656 nm. Nevertheless, photoionization also opens a decay channel for state $|2\rangle$, thus spoiling its metastability. But its decay rate can be kept small compared to that for state $|3\rangle$ by adequately choosing the laser intensities. In the following calculations, the condition $\Gamma_2 \le \Gamma_3$ is always satisfied, maintaining the destructive interference in the linear susceptibility. The intensity of the generated radiation was evaluated by solving the propagation equation as shown in Ref. [8] using the linear and nonlinear susceptibilities convoluted over the Gaussian density of states with an effective Doppler width.

III. EXPERIMENT

A. Laser system

In Fig. 2 the experimental setup used for the present study is shown. An injection-seeded Nd:YAG laser (Spectron Laser Systems SL802G, YAG denotes yttrium

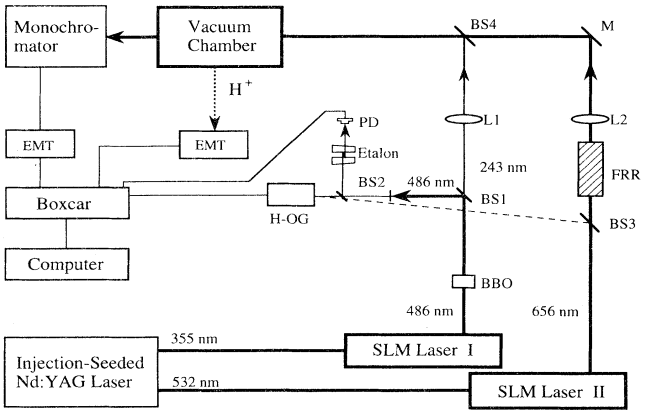

FIG. 2. Schematic diagram of the experimental setup used for the sum-frequency generation in atomic hydrogen. SLM laser, single longitudinal-mode dye laser; BBO, β-barium-borate crystal; BS1–BS4, beam splitters; H-OG, hydrogen optogalvanic lamp; FRR, Fresnel-rhombic retarder; PD, photodiode; M, total-reflection mirror; EMT, electron multiplier.

aluminum garnet) was used to pump two sets of dye lasers. The third harmonic (355 nm) of the Nd:YAG laser was used for dye laser I to generate the 486-nm laser beam for two-photon resonance. The second harmonic (532 nm) was used for dye laser II to generate the 656-nm laser beam for coupling states $|3\rangle$ and $|2\rangle$. Important operating characteristics required for both dye lasers are smooth temporal and spatial profiles, especially for the 656-nm laser used for the strong coupling. Smooth profiles were obtained by operating the two laser oscillators in a single longitudinal mode (SLM) using a grazing-incidence cavity geometry [17,18]. The SLM dye lasers were smoothly tunable by more than 20 cm^{-1} without mode hopping and the beams were amplified through three-stage amplifiers. The amplified output of the 486-nm dye laser was 3 mJ in energy with a pulse width of 4 ns. In terms of the coupling 656-nm laser, the output was raised to 6 mJ with a 5 ns pulse width [full width at half maximum (FWHM)]. Gaussian profiles were maintained in both spatial and temporal distributions after amplification. The pulse-to-pulse power fluctuation of the two lasers was measured to be less than $\pm 15\%$. Linewidths of the SLM 486- and 656-nm lasers were measured to be less than 0.02 cm^{-1} (FWHM) using an air-spaced étalon and the pulse-to-pulse frequency jitter in both lasers was found to be about 0.02 cm^{-1}.

The 486-nm radiation was frequency-doubled by a β-barium-borate (BBO) crystal to 243-nm radiation, with an energy of 0.3 mJ per pulse and a pulse width of 4 ns (FWHM). When the 486-nm laser was scanned, the BBO crystal was tracked to keep the optimum phase-matching condition for stabilizing the energy of the 243-nm laser beam. A Pellin-Broca prism was used to separate the 486- and the 243-nm beams. The 486-nm beam was then attenuated and sent into a H optogalvanic lamp and into an air-spaced étalon. The H optogalvanic lamp was used to calibrate the absolute wavelength of the 486-nm laser through the $n=4$-2 resonance transition, which has a frequency exactly one-fourth of that for the $n=2$-1 transition. The coupling 656-nm beam was fixed to the resonance of the $3p$-$2s$ transition to an accuracy better than ± 0.15 cm^{-1}, throughout the experiments. The polarization of the 656-nm beam was converted to σ^+-circular polarization by a Fresnel rhomb retarder.

The 243- and the 656-nm laser beams were loosely focused by using two lenses with focal lengths of 1 and 1.5 m, respectively, and were overlapped spatially with the use of a dichroic mirror. The two beams were temporally overlapped by adjusting the delay of each laser, although temporal jitter was about ± 0.5 ns, due to the different buildup time of the two laser oscillators. At the focus spot in the interaction region, the respective beam sizes were measured by burning a beam pattern on checking paper: the 656-nm laser beam had a diameter of 0.7 mm and a focal depth of 30 cm and the 243-nm laser beam was 0.5 nm in diameter and 20 cm in focal depth.

B. H-atom generation and signal observation

Figure 3 illustrates the schematic diagram of the atomic hydrogen apparatus. Hydrogen atoms were generated in a microwave discharge at 2.45 GHz, using a cavity developed by Fehsenfeld, Evenson, and Broida (type II) [19]. Microwave power of 40 W was fed to the cavity. A quartz discharge tube was located in the cavity and H_2 gas with purity of 99.999 99% flowed through the discharge tube at pressures between 0.1 and 1 Torr, regulated by a mass-flow controller (STEC Inc. Model DS-3). In order to stabilize the discharge, deionized H_2O vapor at a pressure 0.15 Torr was added to the H_2 gas through a bypass. The quartz tube was coupled to a vacuum chamber by a Teflon block having a linear series of five nozzles, which allowed the generated atoms to diffuse into the vacuum chamber. The five nozzles of 0.5 mm diameter were spaced 7 mm apart. Two optical-quality Pyrex blocks (5 cm long, with spacing of 0.6 mm) were located immediately below the Teflon block to confine the

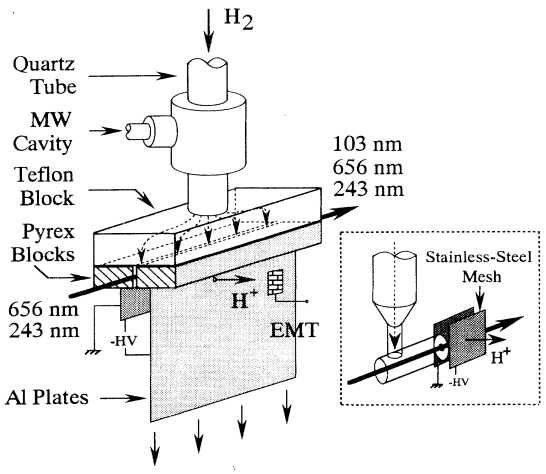

FIG. 3. Schematic diagram of the atomic-hydrogen beam and cell system. The metal plates and mesh are used for extracting the photoions.

atoms from the nozzles through the interaction region. The atomic density was varied by adjusting the H_2 pressure and reached a maximum density in the interaction region estimated to be 2×10^{14} cm^{-3}, using the same procedures described in Ref. [20].

Two parallel aluminum plates with 1-cm spacing were set under the Pyrex blocks for measuring the ions produced by the laser beams. A hole 1 mm in diameter was made in the plate center 2 cm below the interaction region to extract the hydrogen ions by applying a pulsed electric field to the two plates as the ions diffused vertically into the vacuum chamber. We note that the hole allows us to spatially select photoions from a small interaction region. An electric field of 250 V/cm and 2 μs pulse width was applied 1.5 μs after the laser irradiation and the ions were detected with a Hamamatsu-R515 electron multiplier tube (EMT).

In order to achieve higher atomic densities, the gas was confined in a Pyrex cell (3.5 cm long and 1.0 cm in diameter), connected to the discharge tube (Fig. 3, inset). The cell was closed by a quartz window (3 mm thick) at the laser beam entrance end and by a Pyrex window (3 mm thick) with a 1-mm aperture at the vuv exit end. Under these conditions, the maximum density of atomic hydrogen was estimated to be 10^{15} cm^{-3}.

Generated vuv radiation was separated from the incident laser radiation by a monochromator (Acton Research Corporation VM502) with a slit width of 100 μm and detected by an EMT (Hamamatsu R515). For absolute measurement of the generated vuv intensity, we used a windowless photodiode with absolute calibration in the EUV to vuv spectral region (National Bureau of Standards, Serial No. 311). For measurement of the vuv pulse width, a fast response time EMT (Hamamatsu R5600) was used having a nominal rise time of 0.8 ns and a fall time of 1 ns. All signals from the EMT detectors, the H optogalvanic lamp, and the photodiodes were averaged by boxcar integrators (Stanford Research Systems SR250) and processed by a computer.

IV. RESULTS AND DISCUSSION

A. Calculated characteristics

1. *Tuning characteristics: Ω_{23} dependence*

In Fig. 4(a) the calculated characteristics (normalized) of photoion number versus frequency detuning of the two-photon frequency for different coupling Rabi frequencies Ω_{23} are displayed. The density-length product NL is fixed at a value of 7×10^{14} cm^{-2}. At $\Omega_{23}=1$ cm^{-1}, the photoion spectrum appears as a single peak at the center. This means that the atomic hydrogen is opaque for the generated radiation because of relatively weak coupling compared with the Doppler width. With the Rabi frequency increased to 4.4 cm^{-1}, two ion peaks are resolved corresponding to transitions from the ground state to the two upper dressed states. At the split center, the photoion number is reduced to 55% of the peak values. At $\Omega_{23}=6.7$ cm^{-1}, the two photoion peaks are well separated by the strong coupling and the calculated

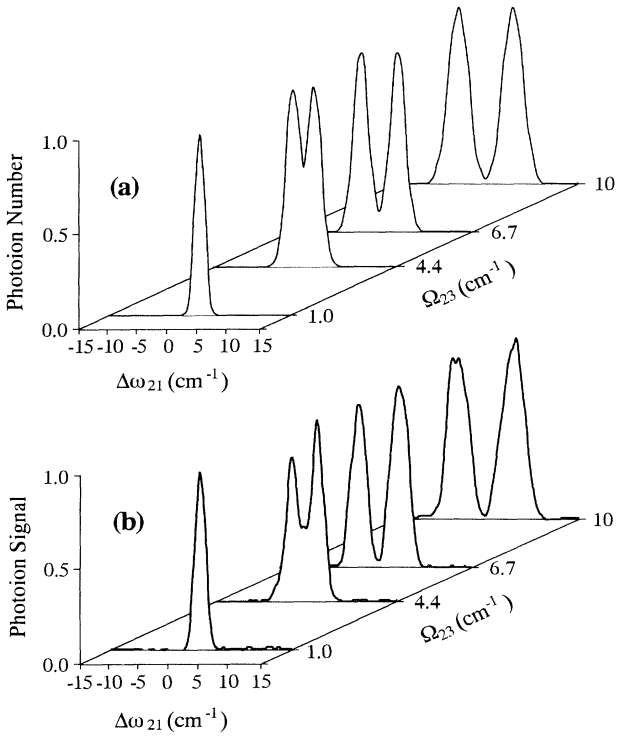

FIG. 4. (a) Calculated tuning characteristics of photoion number versus frequency detuning $\Delta\omega_{21}=\omega_2-2\omega_e$, for coupling Rabi frequencies Ω_{23} of 1–10 cm^{-1}. The density-length product is fixed at 7×10^{14} cm^{-2}. (b) Observed characteristics of photoion signals (normalized to peak values) versus frequency detuning, under the same conditions as in (a).

photoion number at the center is significantly reduced to 10% of the peak values. This reduction results from both the electromagnetically induced transparency and ac Stark splitting, not only the Stark splitting. If EIT is not involved, the calculation leads to a photoionization signal at the center of more than 20% of the peak values. When the coupling strength Ω_{23} is increased to 10 cm^{-1}, the center photoion number is suppressed to 1% of the peak values, clearly indicating the effect of induced transparency.

In Fig. 5(a) the tuning characteristics of the generated radiation versus the frequency detuning $\Delta\omega_{21}$ for different coupling Rabi frequencies are shown, as well as an NL value of 7×10^{14} cm^{-2}. At a Rabi frequency of 1 cm^{-1}, the spectrum exhibits a broad central peak with shoulders corresponding to the dressed-state positions. Although the central peak is slightly higher than the peaks of the dressed states, a strong enhancement is not observed at the center. This behavior results from the strong absorption due to the weak coupling. With Rabi frequency increased to 4.4 cm^{-1}, strong enhancement at the center intensity is seen compared to the intensities at the two dressed states. This strong enhancement is also exhibited in the spectrum with the coupling strength of 6.7 cm^{-1}. Such strong enhancement at the center is the prominent effect arising from the combination of induced

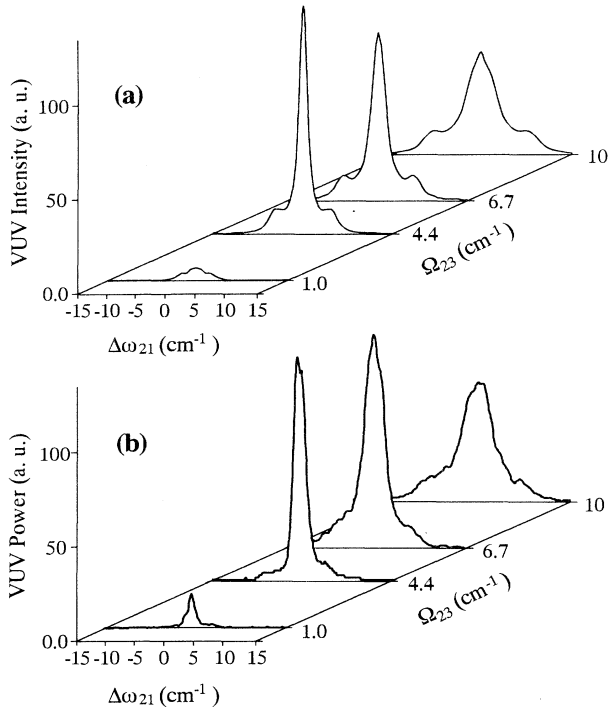

FIG. 5. (a) Calculated tuning characteristics of sum-frequency generation versus frequency detuning $\Delta\omega_{21}=\omega_2-2\omega_e$, for different coupling Rabi frequencies of Ω_{23}. The density-length product is 7×10^{14} cm^{-2}. (b) Observed characteristics of sum-frequency generation versus frequency detuning, under the same conditions as in (a).

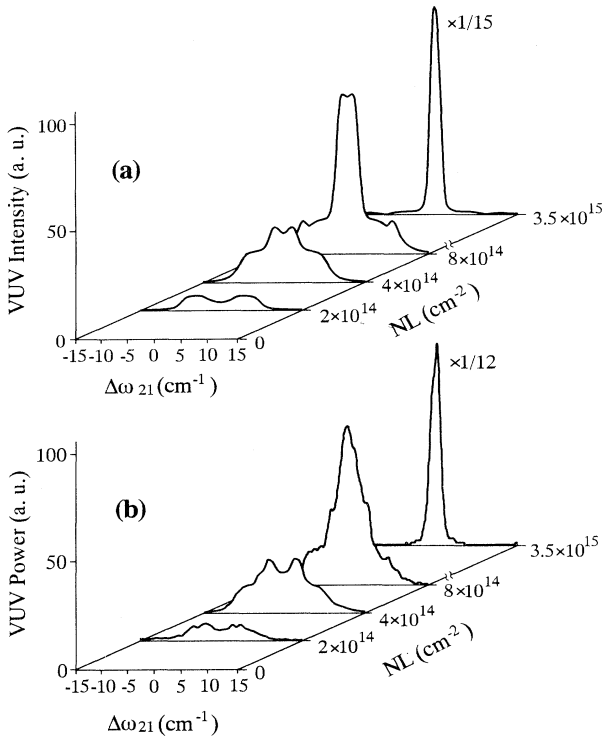

FIG. 6. (a) Calculated tuning characteristics of sum-frequency generation versus frequency detuning $\Delta\omega_{21}=\omega_2-2\omega_e$, for density-length products *NL* of 2.0×10^{14}–3.5×10^{15} cm^{-2}. The coupling Rabi frequency is fixed at 10 cm^{-1}. (b) Observed characteristics of sum-frequency generation versus frequency detuning, under the same conditions as in (a).

transparency and enhanced nonlinear susceptibility. When Ω_{23} is increased to 10 cm^{-1}, the intensity at the center is reduced by a factor of about 2 compared with that at 6.7 cm^{-1} of Ω_{23}. This reduction is due to the fact that, since the absorption at the center has been strongly reduced by the large Rabi frequency of 10 cm^{-1}, the generated intensity, expressed as Eq. (11) of Ref. [8], has not reached a stationary value under the present *NL* condition. Such an intensity reduction may be compensated by using a higher *NL* condition, as shown below.

2. *Tuning characteristics: NL dependence*

The calculated tuning characteristics of the generated radiation for four *NL* values versus the detuning of the two-photon frequency $\Delta\omega_{21}$ are illustrated in Fig. 6(a). The coupling Rabi frequency was fixed at $\Omega_{23}=10$ cm^{-1}. At the relatively low *NL* value of 2×10^{14} cm^{-2}, the spectrum shows two peaks corresponding to the two dressed states. It is important to note that the intensity at the center remains at half of its peak value, even though the photoion number is suppressed almost to zero under the same condition as shown in Fig. 4(a). This profile reflects a typical behavior of the nonlinear susceptibility $\chi_D^{(NL)}(-\omega_g,\omega_e,\omega_e)$; its value maintains a resonant value at the center due to constructive interference [7]. As *NL* is increased up to 3.5×10^{15} cm^{-2}, the intensities at the dressed states are quickly saturated, but the intensity at the center can grow quadratically with *NL*, up to 3.5×10^{15} cm^{-2}. This quadratic enhancement at the center reveals that absorption has been reduced to almost zero at the center and that the phase-matching condition is simultaneously satisfied.

B. Experimental observations

1. *Tuning characteristics: Ω_{23} dependence*

In Fig. 4(b) the observed characteristics of photoion signals versus detuning $\Delta\omega_{21}$ for four different coupling-strengths (Ω_{23}) are shown, as well as an *NL* value estimated to be 7×10^{14} cm^{-2}. The effective coupling strengths were calibrated by measuring the separation of two ion peaks. The observed photoion signals are normalized to their peak values. For the coupling strength of 1 cm^{-1} (at a coupling intensity of 0.5 MW cm^{-2}), the photoion signal shows a single peak at the center. With the strength Ω_{23} increased to 4.4 cm^{-1}, the photoion signal splits into two components and the signal intensity at the split center is reduced to $\sim$50% of the peak values. For an Ω_{23} value of 6.7 cm^{-1}, the center ion signal is

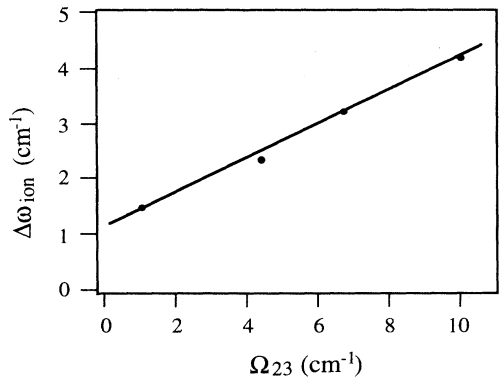

FIG. 7. Widths of photoion signals (FWHM) at dressed-state positions are plotted for different coupling Rabi frequencies of Ω_{23}. The circles show the observed values and the solid line gives the linear fitting.

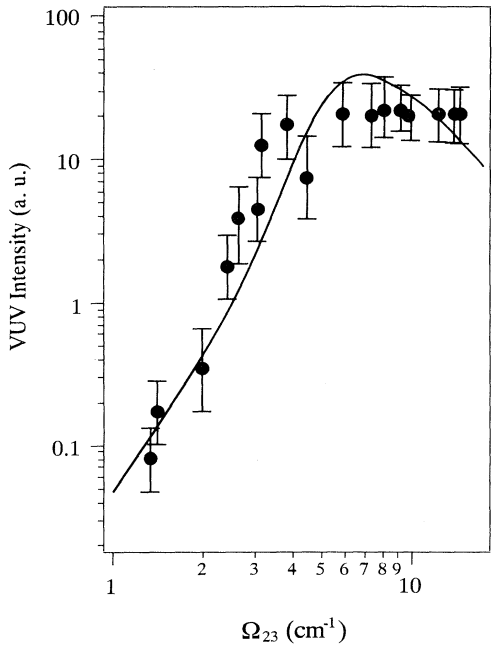

FIG. 8. Intensities of generated radiation at the split center of the two upper dressed states $|3d\rangle$ and $|2d\rangle$ are plotted versus coupling Rabi frequency of Ω_{23}. The observed values are marked by circles with error bars. The solid line denotes the theoretical plot. The density-length product is fixed at 3.5×10^{15} cm^{-2}.

suppressed to 5% of the peak values and for $\Omega_{23}=10$ cm^{-1} the signal at center is suppressed to almost zero. The observed characteristics show excellent agreement with the calculated values in Fig. 4(a), clearly demonstrating the EIT effect, i.e., reduced absorption on resonance.

In the photoion spectra, we can readily see the gradual broadening of the widths as the coupling strength increases. A graph of observed widths (FWHM) versus the coupling strengths plotted in Fig. 7 was fitted by the linear relation $\Delta\omega_{ion}\approx1.2+0.3\Omega_{23}$ (FWHM in cm^{-1}). The width at $\Omega_{23}=0$ corresponds to the Doppler width at room temperature. We have discussed such broadening for strong coupling in the context of depopulation of ground-state atoms [21], but the observed broadening cannot be explained completely by the depopulation effect. In the present case, the origin of the broadening may be attributed mainly to inhomogeneity of the coupling field in both spatial and temporal aspects. Although the temporal and spatial widths of the coupling laser beam exceed those of the 243-nm beam, an inhomogeneity of 10% for each may be inevitable and can lead to the observed increase of the width proportional to effective coupling strength. Thus we have treated this broadening as inhomogeneous broadening of the present system.

The observed tuning characteristics of the generated vuv radiation are shown in Fig. 5(b). A single peak at the center is clearly seen for each spectrum. For coupling strength from 1 to 4.4 cm^{-1}, the intensity at the center grows rapidly and a further increase results in a decrease of the central peak with broadening of its width. These observed characteristics reproduce in detail the calculated spectra shown in Fig. 5(a).

The generated intensities at line center versus coupling strength Ω_{23} and for an NL value of 3.5×10^{15} cm^{-2} are plotted in Fig. 8. The data are displayed on a logarithm scale for both intensity and coupling strength. It is seen that the calculated line explains the observed behavior. The generated vuv signal builds up very quickly when the coupling Rabi frequency exceeds the Doppler width of 1.2 cm^{-1} (FWHM) and creates the transparency at line center while satisfying the phase-matching condition. An enhancement by a factor for 250 was obtained by increasing Ω_{23} from 1.4 to 7 cm^{-1}.

2. *NL dependence*

In Fig. 6(b) the observed tuning characteristics of the generated radiation versus detuning $\Delta\omega_{21}$ for four different NL values are shown with the coupling strength Ω_{23} fixed at 10 cm^{-1}. The spectra at $NL=2\times10^{14}$ and 4×10^{14} cm^{-2} show a two-peak structure, reflecting the profiles of the dressed nonlinear susceptibility. When the NL value was raised to 8×10^{14} cm^{-2}, the intensity at line center increased by a factor 16, a quadratic enhancement with the increase of the NL value. At $NL=3.5\times10^{15}$ cm^{-2}, the intensity at the center increased about 200 times compared with that at 2×10^{14} cm^{-2}. Again, the observed results are in good agreement with the calculated spectra of Fig. 6(a).

The observed and calculated intensities at line center and at the dressed-state positions versus the density-length product are plotted in Fig. 9. It is seen that, although the intensities at the dressed states are quickly saturated by strong absorption as NL is raised, the center intensity continues to grow quadratically with an increase in NL to 3.5×10^{15} cm^{-2}. The quadratic increase at line center together with the suppressed ion signal clearly demonstrates that the present atomic hydrogen scheme

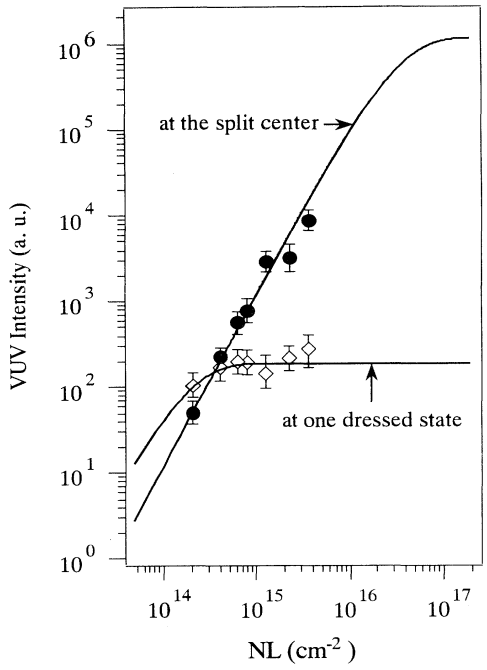

FIG. 9. Intensities of the generated radiation both at the split center and at one of the two dressed states are plotted versus the density-length product NL. The coupling intensity is fixed at an effective Rabi frequency of 10 cm^{-1}. The circles show the intensities at the split center and the rhombic markers display the intensities at the dressed state. Solid lines are the theoretical curves.

confirms the reduced absorption and the induced phase matching under the strong-coupling condition and that the nonlinear susceptibility maintains the resonant enhancement, thus revealing a completely different behavior from the linear susceptibility. The experimental results show excellent agreement with the calculated values up to the NL value of 3.5×10^{15} cm^{-2}, the maximum value attainable in the present experiments.

At this maximum NL value, the energy of generated 103-nm radiation was measured to be 68 nJ, with a pulse width of $\sim$3 ns and beam diameter of 0.3 mm. These parameters give a generated power of 3.3 W per pulse with a conversion efficiency η of $\sim2\times10^{-4}$ in the power of the two-photon, 243-nm beam. Under the present conditions, the conversion efficiency can be calculated simply as proportional to $|\chi_D^{(NL)}|^2$ yielding a value of 2.4×10^{-4}, in excellent agreement with the observed value. In terms of an input energy of 0.4 mJ at 243 nm, this conversion efficiency is considered to be a large value for generation of vuv radiation at $\sim$100 nm. Although the peak power of generated vuv radiation at 103 nm was limited by the presently attainable experimental conditions, the calculations predict a quadratic increase by two orders of magnitude in power and efficiency, for an NL value of $\sim10^{17}$ cm^{-2}, when the final restriction due to residual absorption sets in.

V. CONCLUSIONS

We have systematically analyzed the sum-frequency generation process using strong-field coupling and quantum interference for the generation of coherent vuv radiation using atomic hydrogen as a test medium. It has been shown that coupling of the $1s$ ground and the $2s$ metastable states by two-photon resonance and simultaneous strong coupling of the $3p$ and $2s$ states, creates destructive interference to reduce the linear susceptibility at the $3p\leftarrow1s$ transition, as well as constructive interference to resonantly enhance the nonlinear susceptibility for sum-frequency generation of coherent Lyman-β radiation ($3p\rightarrow1s$) at 103 nm. Theoretical calculations of the interaction were carried out based on a dressed-state treatment including the effects of photoionization from the upper states.

Experimental results have confirmed the theoretical predictions. When the coupling Rabi frequency exceeds the Doppler broadening of the medium, the photoion signals at the resonant center are suppressed significantly and the generated Lyman-β radiation has grown rapidly by a factor 250 at an atom density of 1×10^{15} cm^{-3} and an interaction length of 3.5 cm, resulting in a conversion efficiency of 2×10^{-4}. The excellent agreement between theory and experiment indicates the possibility of enhancing the conversion efficiency by another two orders of magnitude by increasing the interacting atom-density length product. While the present work has demonstrated the possibility of nonlinear optical generation using strong-field coupling and interference in the atomic hydrogen, this concept should be applicable to other atomic and molecular systems, as well as fabricated quantum-well structures, and may open new possibilities for generating short-wavelength coherent radiation.

ACKNOWLEDGMENTS

The authors thank Professor S. E. Harris for kindly arranging the loan of the calibrated EUV photodiode. They also thank M. Ohta and S. Yoshida for helpful discussions and assistance in the experiments. One of the authors (G.Z.Z.) is grateful to the Ministry of Education of Japan and another (R.I.T.) to the Natural Sciences and Engineering Research Council of Canada (NSERCC) for financial support during the course of this study. This work was supported by the Grant-in-Aid for scientific research from the Ministry of Education of Japan, by Matsuo Foudation, by NSERCC, and by the Ontario Technology Fund.

[1] D. C. Hanna, M. A. Yuratich, and D. Cotter, *Nonlinear Optics of Free Atoms and Molecules* (Springer-Verlag, Berlin, 1979); P. N. Butcher and D. Cotter, *The Elements of Nonlinear Optics* (Cambridge University Press, Cambridge, 1990).

[2] R. Hilbig, G. Hilber, A. Lago, B. Wolf, and R. Wallenstein, Comments At. Mol. Phys. **18**, 157 (1986); C. R. Vidal, in *Tunable Lasers,* edited by L. F. Mollenauer and J. C. White (Springer-Verlag, Heidelberg, 1984), p. 57; W. Jamroz and B. P. Stoicheff, in *Progress in Optics XX,* edited by E. Wolf (North-Holland, Amsterdam, 1983), p. 325.

[3] S. E. Harris, J. E. Field, and A. Imamoglu, Phys. Rev. Lett. **64**, 1107 (1990).

[4] A. Imamoglu and S. E. Harris, Opt. Lett. **14**, 1344 (1989).

[5] K.-J. Boller, A. Imamoglu, and S. E. Harris, Phys. Rev. Lett. **66** 2593 (1991).

[6] J. E. Field, K. H. Hahn, and S. E. Harris, Phys. Rev. Lett. **67**, 3062 (1991).

[7] K. Hakuta, L. Marmet, and B. P. Stoicheff, Phys. Rev. Lett. **66**, 596 (1991).

[8] K. Hakuta, L. Marmet, and B. P. Stoicheff, in *Laser Spectroscopy X,* edited by M. Ducloy, E. Giacobino, and G. Camy (World Scientific, Singapore, 1991), p. 301.

[9] K. Hakuta, L. Marmet, and B. P. Stoicheff, Phys. Rev. A **45**, 5152 (1992).

[10] K. H. Hahn, D. A. King, and S. E. Harris, Phys. Rev. Lett. **65**, 2777 (1991).

[11] M. O. Scully and M. Fleischhauer, Phys. Rev. Lett. **69**, 1360 (1992); M. Jain, G. Y. Yin, J. E. Field, and S. E. Harris, Opt. Lett. **18**, 998 (1993); S. E. Harris, *ibid.* **19**, 2018 (1994).

[12] G. Z. Zhang, K. Hakuta, and B. P. Stoicheff, Phys. Rev. Lett. **71**, 3099 (1993).

[13] S. E. Harris, Phys. Rev. Lett. **62**, 1033 (1989).

[14] I. I. Sobelman, *Atomic Spectra and Radiative Transitions* (Springer-Verlag, New York, 1979).

[15] A. Burgess, Mem. R. Astron. Soc. **69**, 1 (1965).

[16] E. U. Condon and G. H. Shortley, *Theory of Atomic Spectra* (Cambridge University Press, Cambridge, 1987), p. 136.

[17] M. G. Littman, Opt. Lett. **3**, 138 (1978); K. Liu and M. G. Littman, *ibid.* **6**, 117 (1981); M. G. Littman, Appl. Opt. **23**, 4465 (1984).

[18] G. Z. Zhang and K. Hakuta, Opt. Lett. **17**, 997 (1992).

[19] F. C. Fehsenfeld, K. M. Evenson, and H. P. Broida, Rev. Sci. Instrum. **36**, 294 (1965).

[20] L. Marmet, K. Hakuta, and B. P. Stoicheff, J. Opt. Soc. Am. B **9**, 1038 (1992).

[21] R. I. Thompson, B. P. Stoicheff, G. Z. Zhang, and K. Hakuta, Quantum Opt. **6**, 349 (1994).